Atmospheric Environment 89 (2014) 158–168

Contents lists available at ScienceDirect

Atmospheric Environment

journal homepage: www.elsevier.com/locate/atmosenv

The role of temporal evolution in modeling atmospheric emissions from tropical fires

Miriam E. Marlier [a,*], Apostolos Voulgarakis [b], Drew T. Shindell [c], Greg Faluvegi [c], Candise L. Henry [a], James T. Randerson [d]

[a] Lamont-Doherty Earth Observatory and Dept. of Earth and Environmental Sciences at Columbia University, USA
[b] Dept. of Physics, Imperial College London, UK
[c] NASA Goddard Institute for Space Studies, USA
[d] Dept. of Earth System Science, University of California, Irvine, USA

HIGHLIGHTS

- Daily and monthly resolution GFED fire emissions were modeled with GISS-E2-PUCCINI.
- Simulations with daily resolution emissions were better timed with meteorology.
- Effects on simulations of air quality exceedances and atmospheric heating patterns.

ARTICLE INFO

Article history:
Received 8 October 2013
Received in revised form
14 February 2014
Accepted 18 February 2014
Available online 19 February 2014

Keywords:
Fire emissions
Atmospheric modeling
Air quality

ABSTRACT

Fire emissions associated with tropical land use change and maintenance influence atmospheric composition, air quality, and climate. In this study, we explore the effects of representing fire emissions at daily versus monthly resolution in a global composition-climate model. We find that simulations of aerosols are impacted more by the temporal resolution of fire emissions than trace gases such as carbon monoxide or ozone. Daily-resolved datasets concentrate emissions from fire events over shorter time periods and allow them to more realistically interact with model meteorology, reducing how often emissions are concurrently released with precipitation events and in turn increasing peak aerosol concentrations. The magnitude of this effect varies across tropical ecosystem types, ranging from smaller changes in modeling the low intensity, frequent burning typical of savanna ecosystems to larger differences when modeling the short-term, intense fires that characterize deforestation events. The utility of modeling fire emissions at a daily resolution also depends on the application, such as modeling exceedances of particulate matter concentrations over air quality guidelines or simulating regional atmospheric heating patterns.

1. Introduction

Fires are widely used throughout the tropics to create and maintain areas for agricultural systems, but are also significant contributors to atmospheric trace gas and aerosol concentrations (Andreae and Merlet, 2001). Emissions associated with deforestation averaged 1 Pg carbon per year over the past decade (Baccini et al., 2012), while also adding to atmospheric ozone (O_3) precursors such as carbon monoxide (CO), nitrogen oxides (NO_x) and VOCs, sulfur-containing compounds, and particulates (Langmann et al., 2009). In addition to the diversity in the type of emissions, the timing and magnitude of fire activity also varies interannually and by biome. This suggests that representing fire emissions at different temporal resolutions in atmospheric models could alter interactions between emissions and atmospheric chemistry and transport, which also vary significantly on several timescales.

The tropics comprise a critical region for global fire activity, but have varying fire behavior characteristics (van der Werf et al., 2010). Frequent but lower intensity fires are typical in savanna areas in Africa and South America (van der Werf et al., 2010). Fire emissions from Southern Hemisphere Africa are dominated by savanna burning, but the Amazon includes a mix of savanna and deforestation fires, which leads to higher rates of fuel consumption and fewer fire days per year (when emissions are aggregated at a 0.5°

* Corresponding author.
E-mail addresses: marlier@ldeo.columbia.edu, miriammarlier@gmail.com (M. E. Marlier).

http://dx.doi.org/10.1016/j.atmosenv.2014.02.039
1352-2310/

spatial resolution). Equatorial Asia has even fewer average fire days per year and higher daily rates of fuel consumption (Mu et al., 2011). On longer timescales, carbon-rich Equatorial Asian peatland forest fires have higher interannual variability than other biomes (van der Werf et al., 2010), with large pulses of emissions during El Niño droughts (van der Werf et al., 2008). These regional differences in emissions characteristics suggest that fire emissions inventories with monthly resolution may be able to adequately resolve dominant modes of variability of fire behavior in certain biomes, but could be insufficient in other areas. An important challenge for the atmospheric sciences community is to understand how this variability in fire behavior influences chemistry, radiative forcing, and air quality.

Monthly global gridded fire emissions inventories typically combine information from satellite observations of burned area, active fire detections, underlying vegetation characteristics, and meteorology. One example is the Global Fire Emissions Database version 3 (GFED3), which is available at a monthly resolution from 1997 to 2011 (van der Werf et al., 2010). From November 2000 onwards, it detects changes in 500-m Moderate Resolution Imaging Spectroradiometer (MODIS) surface reflectance and 1-km MODIS active fires to inform an automated hybrid burned area mapping algorithm (Giglio et al., 2009). Before 2000, active fire detections from Tropical Rainfall Measuring Mission (TRMM) Visible and Infrared Scanner (VIRS) and the Along-Track Scanning Radiometer (ATSR) are used to estimate burned area by means of a regression with MODIS burned area during overlap periods, which necessitates the dataset's monthly resolution (Giglio et al., 2010). Duncan et al. (2003) used active fire data from ATSR and the Advanced Very High Resolution Radiometer (AVHRR) to estimate seasonal fire variability, with the Total Ozone Mapping Spectrometer (TOMS) Aerosol Index serving as a proxy for interannual variability in selected regions, which then scaled an existing biomass burning inventory. While these datasets capture important information on seasonal and interannual variability in fire activity, they may have important limitations when implemented into modeling systems which otherwise operate at sub-daily increments.

Recognizing these potential limitations, several fire emissions inventories at daily or sub-daily resolution are also available, using satellite active fire detections to represent emissions at a finer temporal resolution. Mu et al. (2011) recently applied active fire counts from MODIS and the Geostationary Operational Environmental Satellite (GOES) Wildfire Automated Biomass Burning Algorithm (WF_ABBA) to create daily and 3-hourly emissions inventories, respectively, from the original GFED3 monthly dataset. Heald et al. (2003) applied AVHRR active fire observations to the Duncan et al. (2003) inventory to create a daily emissions dataset for early 2001. The Fire Inventory from NCAR (FINN) is a daily 1-km global dataset of trace gas and particulate emissions from fires, available from 2005 to 10 (Wiedinmyer et al., 2011). FINN primarily uses MODIS active fire detections, an assumed burned area per detection (to allow the product to be released close to real-time), and MODIS land cover types to estimate fuel loadings. Fire Locating and Modeling of Burning Emissions (FLAMBE) combines GOES WF_ABBA, near real-time MODIS active fire products, and 1-km AVHRR land cover maps to create hourly emissions inventories, from 2005 onwards (Reid et al., 2009). Kaiser et al. (2012) developed the 0.5 × 0.5° Global Fire Assimilation System (GFASv1.0), available from 2003, by calculating biomass burning emissions based on MODIS fire radiative power and land cover-specific combustion factors derived from the GFED3 emissions inventory.

Many daily or sub-daily emissions products rely on MODIS active fire detections and are therefore only available since late 2002, when both Terra and Aqua were in operation together. Therefore, for modeling studies before the MODIS era, monthly inventories may still be the only option. Some chemical transport models are moving towards using daily or hourly fire emissions (Mu et al., 2011), although most global composition-climate models currently implement monthly resolution emissions (Lee et al., 2013). It remains unclear which aspects of atmospheric modeling are most sensitive to this choice of temporal resolution, because in previous studies, using finer temporal resolution emissions over coarser resolution datasets have offered variable improvements when compared with observations. Model simulations focusing on CO have found improvements with daily over monthly fire emissions but not sub-daily resolution emissions (Mu et al., 2011), monthly over climatological, but not daily (Heald et al., 2003), and 8-day instead of monthly, but not diurnal (Chen et al., 2009). Simulations of shorter-lived species like NO_2 improve from sub-daily emissions that capture the afternoon peak of biomass burning emissions (Boersma et al., 2008). In boreal North America, Chen et al. (2009) found that aerosols were more sensitive to using 8-day versus monthly resolution emissions than was found with CO (also without further improvements with diurnal resolution). In areas such as Singapore, where biomass burning aerosol transport from Indonesia is highly variable over the fire season, both with respect to shifts in geographic patterns of burning and atmospheric transport patterns, detailed temporal resolution of fire emissions inventories may improve modeled regional aerosol concentrations (Atwood et al., 2013). Modeling the interactions between smoke aerosols by changing absorption patterns of radiation can also vary strongly on sub-daily timescales (Wang and Christopher, 2006; Wu et al., 2011).

In this study, we examine the sensitivity of multiple endpoints to using daily and monthly resolution fire emissions: modeling trace gases and aerosols, assessing air quality and public health effects, and estimating climate impacts. We hypothesize that changing from monthly to daily fire emissions will: 1) produce a varied response throughout the tropics, depending on biome-specific fire behavior (for example, continuous low intensity fires would lead to smaller atmospheric differences in savanna regions), 2) allow for higher peak concentrations since short-lived fire events can be concentrated over several days and not averaged over a month, and 3) more realistically synchronize emissions with meteorology, with fires predominately occurring on sunny, precipitation-free days, which would lower wet deposition of aerosols and could increase the speed of some chemical reactions. Section 2 describes the model framework and observational datasets; Section 3 presents our results for atmospheric composition, air quality, and radiative forcing; Section 4 describes our conclusions.

2. Materials and methods

2.1. Model set-up

Baseline monthly fire emissions estimates were from GFED3, which combines surface reflectance and active fire detections from several satellites to detect the spatiotemporal variability of burned area (Giglio et al., 2010). This drives a biogeochemical model that estimates fuel loads, combustion completeness, and emissions (van der Werf et al., 2010). GFED3 is available for 1997 onwards at 0.5° × 0.5° horizontal resolution. This dataset comprised the fire input for our monthly fire emissions (MF) run.

To isolate the influence of the temporal resolution of fire emissions instead of variations among fire emissions inventories, we used a daily emissions dataset with the same bulk total emissions as the monthly GFED3 dataset. Mu et al. (2011) used MODIS active fire detections aboard the Terra and Aqua satellites to parse the monthly GFED3 emissions to a daily resolution. Due to gaps in

satellite overpasses in the tropics, they applied a three day smoothing filter between 25°N and 25°S. This dataset comprised our daily fire emissions (DF) run. Both fire emissions datasets are publicly available (http://www.globalfiredata.org). We did not include diurnal variability in fire emissions.

Simulations were run with GISS-E2-PUCCINI, which is the latest version of the NASA GISS ModelE climate model, including interactive chemistry and aerosols (Shindell et al., 2013b). Following a two year spin-up, it was run at 2° × 2.5° resolution with 40 vertical layers from 2005 to 2009. We conducted three simulations: 1) MF, 2) DF, and 3) NF (no fire emissions).

Our simulations included interactive constituents in the PUCCINI model for chemistry, aerosols (sulfate, carbonaceous, nitrate, dust and sea salt), and an aerosol indirect effect parameterization (Koch et al., 2006; Shindell et al., 2013b). GFED3 emissions were mixed uniformly through the boundary layer. Infrastructure has recently been developed in the PUCINNI model to study pulses of emissions from individual fire events and preliminary results show satisfactory performance compared with observations (Robert Field, personal communication). Monthly emissions were linearly interpolated to daily values for the MF simulation while the daily fractions from the Mu et al. (2011) product were used for the DF simulation. Annually and monthly-varying GFED3 emissions were used for CO, ammonia, black carbon (BC), organic carbon (OC), sulfur dioxide, non-methane hydrocarbons, and NO_x. To isolate the difference between DF and MF, we did not scale aerosol emissions by satellite observations. Present-day anthropogenic emissions were re-gridded to 2° × 2.5° spatial resolution based on Lamarque et al. (2010), which was produced to provide input to models being run in support of the IPCC Fifth Assessment Report (AR5). Methane in the lowest model layer was kept to observed values for each year and lightning NO_x was generated internally based on an updated version of Price et al. (1997). Climate-sensitive isoprene emissions were based on Guenther et al. (1995, 2006); vegetation alkene and paraffin emissions from the GEIA dataset are based on Guenther et al. (1995). Model winds were linearly relaxed towards reanalysis based on meteorological observations (Rienecker et al., 2011). Sea-surface temperatures and sea ice were from monthly observational datasets (Rayner et al., 2003).

We focused on several key trace gases and aerosol species to illustrate the changes between the DF and MF simulations. Trace gases included CO, O_3, and OH to understand how the model simulates atmospheric composition; both O_3 and CO are major pollutants, while O_3 and OH are also directly and indirectly important, respectively, to climate. For aerosols, we focused on BC and OC, which are the main components of particulate matter to which fire emissions contribute (Andreae and Merlet, 2001).

2.2. Ground and satellite observations

We compared model output with ground-based (Table 1) and satellite measurements of O_3, CO, and aerosol optical depth (AOD). Observations were generally selected within primary tropical fire regions as defined in by GFED (van der Werf et al., 2010): Southern Hemisphere South America, Southern Hemisphere Africa, and Equatorial Asia, although we expanded the regions slightly depending on station coverage. Of the 14 GFED regions, these three

Table 1
Description of ground-based validation data for intercomparison with model simulations. WDCGG= World Data Centre for Greenhouse Gases, AERONET = Aerosol Robotic Network, AOD = Aerosol Optical Depth, SHSA=Southern Hemisphere South America, SHAF=Southern Hemisphere Africa, EQAS = Equatorial Asia. Time period lists data beginning and ending dates, irrespective of gaps.

Source	Species	Region	Location (latitude, longitude)	Time period
WDCGG	CO	SHSA	Arembepe, Brazil (−12.8, −38.2)	10/2006–12/2009
	CO, O_3	SHSA	Ushuaia, Argentina (−54.8, −68.3)	3/2005–1/2009
	O_3	SHSA	San Lorenzo, Paraguay (−25.4, −57.6)	3/2005–10/2007
	CO, O_3	SHAF	Cape Point, South Africa (−34.4, 18.5)	CO: 1/2007–12/2009 O_3: 1/2005–12/2009
	CO, O_3	SHAF	Mt. Kenya, Kenya (−0.1, 37.3)	CO: 1/2005–5/2006 O_3: 3/2005–5/2006
	CO	SHAF	Gobabeb, Namibia (−23.6, 15.0)	8/2006–12/2009
	CO, O_3	EQAS	Bukit Koto Tabang, Indonesia (-0.2, 100.3)	CO: 1/2005–12/2009 O_3: 1/2005–12/2007
	O_3	EQAS	Danum Valley, Malaysia (5.0, 117.8)	1/2007–5/2008
AERONET	AOD	SHSA	Abracos Hill (−10.8, −62.4)	1/2005–10/2005
			Alta Floresta (−9.9, −56.1)	1/2005–12/2009
			Belterra (−2.6, −55.0)	1/2005–4/2005
			Campo Grande (−20.4, −54.5)	1/2005–12/2009
			Cuiba Miranda (−15.7, −56.0)	1/2005–6/2009
			Petrolina Sonda (−9.4, −40.5)	1/2005–9/2009
			Rio Branco (−10.0, −67.9)	1/2005–12/2009
			Santa Cruz (−17.8, −63.2)	2/2005–12/2009
			Santa Cruz Utepsa (−17.9, −63.2)	9/2006–11/2008
			Sao Paulo (−23.6, −46.7)	1/2005–12/2009
	AOD	SHAF	ICIPE-Mbita (−0.4, 34.2)	3/2006–8/2008
			Ilorin (8.3, 4.3)	1/2005–12/2009
			Kibale (0.6, 30.4)	12/2006–1/2007
			Mongu (−15.3, 23.2)	1/2005–12/2009
			Nairobi (−1.3, 36.9)	12/2005–6/2009
			Niamey (13.5, 2.2)	8/2006–1/2007
			Skukuza (−25.0, 31.6)	1/2005–12/2009
	AOD	EQAS	Jabiru (−12.7, 132.9)	5/2005–12/2009
			Bandung (−6.9, 107.6)	5/2009–12/2009
			Puspiptek (−6.4, 106.7)	8/2007–11/2007
			Singapore (1.3, 103.8)	11/2006–12/2009
			Bac Lieu (9.3, 105.7)	5/2006–7/2009
			ND Marbel University (6.5, 124.8)	12/2009
			Songkhla (7.2, 100.6)	1/2007–12/2009

contributed more than 50% of global emissions over 2005–2009 (van der Werf et al., 2010).

The World Data Centre for Greenhouse Gases (WDCGG) maintains station trace gas observations (http://ds.data.jma.go.jp/gmd/wdcgg/). We used 24-h averages of surface O_3 and CO concentrations for comparison with surface model output. As described in Table 1, CO and/or O_3 data were available from 8 stations for variable time periods within 2005–2009.

NASA's AErosol RObotic NETwork (AERONET) is a global ground-based sun photometer network (http://aeronet.gsfc.nasa.gov) (Holben et al., 1998). Column AOD is calculated from direct solar radiation measurements. We used Version 2, Level 2.0 24-h average data, which is the highest quality screened product available. There were 24 available stations (Table 1).

We also compared modeled AOD with MODIS and Multi-angle Imaging SpectroRadiometer (MISR) daily satellite AOD products. We averaged modeled instantaneous AOD values for 12pm and 3pm to correspond with the 1:30pm Aqua satellite overpass for MODIS and 9am to 12pm to correspond with the 10:30am Terra satellite overpass for MISR. AOD retrievals from MODIS take advantage of a wide spectral range, daily coverage of the globe, and high spatial resolution. We used the daily MODIS $1^\circ \times 1^\circ$ Level 3, Collection 5 monthly AOD (MOD08 D3) product (http://modis.gsfc.nasa.gov). MISR (http://www-misr.jpl.nasa.gov) simultaneously observes the Earth at nine different angles and four spectral bands, with global coverage every nine days at the equator. We used the gridded $0.5^\circ \times 0.5^\circ$ Level 3 daily AOD product (MIL3DAE) from the green (555 nm) band.

2.3. Air quality

The World Health Organization (WHO) combines results from epidemiological studies on the public health risks of air pollutants and publishes air quality guidelines (World Health Organization, 2006). These guidelines serve as goals for countries to improve air quality, and are published along with higher interim targets levels (ITs) that have additional expected health risks. We examined how modeling population exposure in the tropics changed with DF versus MF by testing changes in peak concentrations through exceedances over 24-h and annual $PM_{2.5}$ and 8-h maximum O_3 ITs.

Annual cardiovascular disease (CVD) mortality burdens were estimated for exposure to fire $PM_{2.5}$ with a power–law relationship that describes how relative risk (RR) changes over a baseline value of 1:

$$\mathrm{RR} = 1 + \alpha(I^{*}C)^{\beta} \quad (1)$$

We used published values for α and β from a reanalysis of studies that include exposure to ambient air pollution, second-hand smoke, and cigarette smoke. For CVD disease, $\alpha = 0.2685$ and $\beta = 0.2730$ (Pope et al., 2011). Annual average total mass $PM_{2.5}$ surface concentrations were used for (C), assuming a constant average inhalation rate (I) of 18 m^3/day to convert to $PM_{2.5}$ dose (in mg). The attributable fraction (AF) and annual mortality (ΔM) were estimated by Ostro (2004):

$$\mathrm{AF} = (\mathrm{RR} - 1)/\mathrm{RR} \quad (2)$$

$$\Delta M_{\mathrm{annual}} = M_b^{*} P * \left(\mathrm{AF}_{\mathrm{fire}} - \mathrm{AF}_{\mathrm{nofire}}\right) \quad (3)$$

where the average annual baseline mortality rate (M_b) was calculated from adult deaths due to cardiovascular disease, averaged over the countries within each region (WHO, 2011). The fraction of people over 30 years was from the UN Population Division (UN, 2011) and baseline population was from CIESIN's Gridded Population of the World version 3 for 2005 (CIESIN, 2005a) and Future Estimates for 2010 (CIESIN, 2005b); both the adult fraction and population were linearly interpolated from 5 yearly to annual estimates. In addition, we estimated the mortality burden due to daily exposure to fire emissions, summed over each year. Here we used a linear concentration-response function between all-cause mortality and PM_{10} exposure (0.8% per 10 $\mu g/m^3$ increase in PM_{10}) with an upper effect threshold of 125 $\mu g/m^3$ (Ostro, 2004). We assumed that the annual mortality rates described previously were evenly spread over the year.

2.4. Radiative forcing

To evaluate the potential climate implications of our results, we calculated differences between surface and top-of-atmosphere (TOA) instantaneous long-wave and shortwave radiative forcing for several constituents affected by biomass burning. Radiative forcing, in W/m^2, was evaluated for BC, O_3, and sulfate (SO_4) in each simulation, as these are the most radiatively active species that are affected by fires. Radiative forcing was calculated online as an average over time during the simulations; calculations were performed twice at each point in time, with the only difference in the two calculations being the constituent field (e.g. BC, O_3, etc.). The radiative forcing calculations follow standard methodology that has been used in previous work with the PUCCINI model (Shindell et al., 2013b; Voulgarakis et al., 2013b).

3. Results

3.1. Atmospheric composition

3.1.1. Aerosols

Fig. 1a shows the difference in the 2005–09 average of surface carbonaceous aerosols (BC + OC) between the DF and MF simulations (Fig. S1 shows relative differences). There was a mixed response in South America (within ±10%), with increases from the DF simulation in western and interior regions of the Amazon, and decreases across savanna regions in the south and east. In Africa, daily emissions increased surface concentrations across tropical forests in the Congo basin, but decreased concentrations closer to source regions in savannas north and south of the equator (within ±10%). DF also led to increased transport of aerosols from Africa to the tropical North Atlantic (+20%). In Equatorial Asia, the differences were the strongest in Borneo and to the north of Borneo (up to +30%), while staying within −10% over source regions in Sumatra. In general, the spatial patterns across the three continents were consistent with reduced surface concentrations near source regions and enhanced long-range transport of aerosols into more remote regions.

We compared modeled aerosol concentrations with ground and satellite observations. Linear correlations (R^2) between 24-h model and AERONET AOD are described in Tables 1 and 2; correlations generally improved with DF over MF. It is important to note that AERONET stations had variable temporal coverage over 2005–09 and were located at a range of distances from fire activity. When we limited results to sites that had correlations between modeled concentrations and observations that were significant at the 0.05 level and with $R^2 > 0.1$ (for both simulations), there were improvements in 5 out of 6 South American stations, 4 out of 5 African stations, and 0 out of 2 Equatorial Asian stations (for DF versus MF). The NF correlations suggested how much fires contribute to AOD at each site. When fire emissions were excluded (NF), the statistically significant stations with $R^2 > 0.1$ decreased on average from R^2 of 0.47 to 0.07 for DF to NF for South America, from 0.28 to 0.12 for

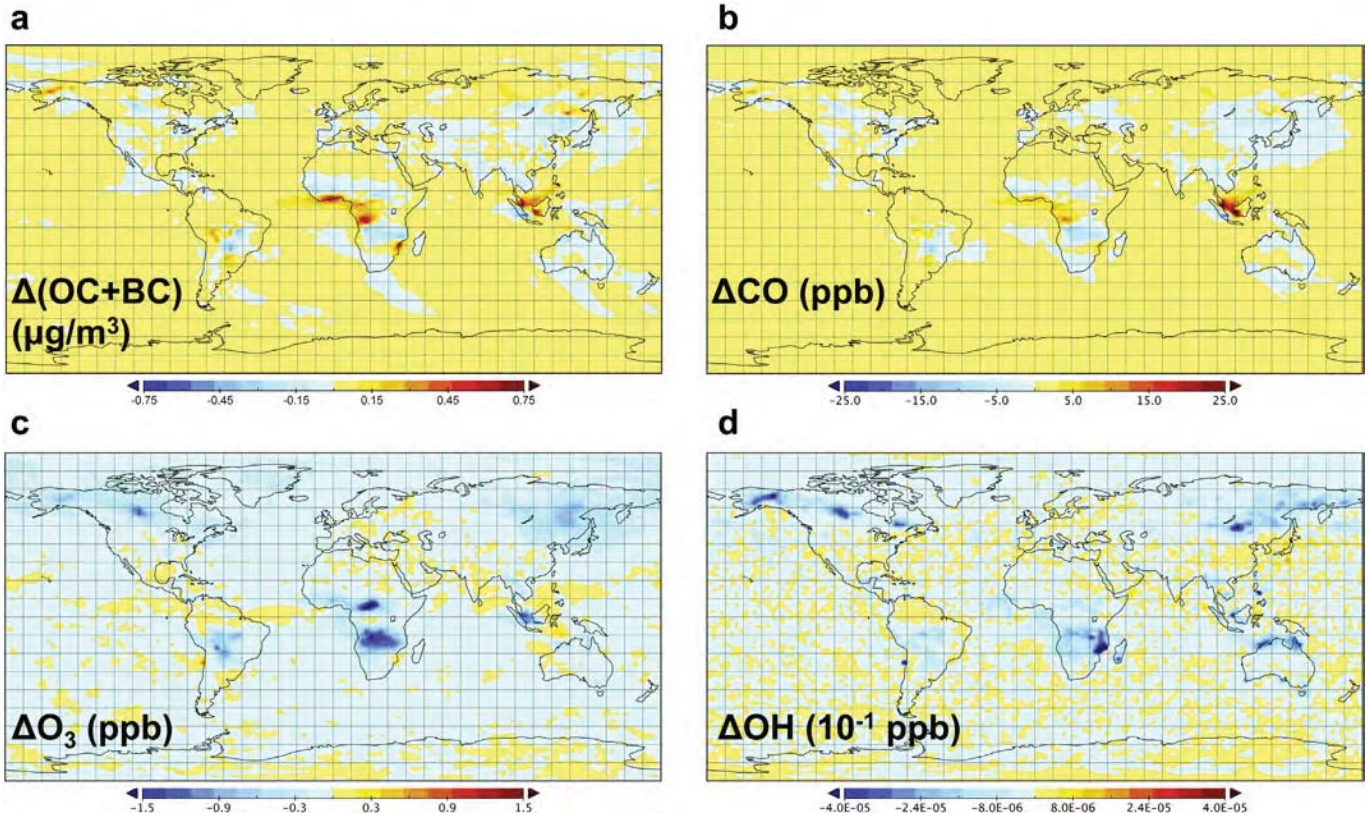

Fig. 1. 2005–09 average differences for surface aerosol and trace gas concentrations (DF – MF emissions global model runs), including all biomass burning sources. a) Carbonaceous aerosols (OC + BC), b) carbon monoxide (CO), c) ozone (O_3), and d) the hydroxyl radical (OH).

Africa, and from 0.14 to 0.08 for Equatorial Asia. Aside from fire emissions, other emissions were not resolved at the daily scale. This can explain some of the low observed correlations, since grid cells in or near cities, for example, could have clear differences in weekday versus weekend emissions due to changes in vehicle and industry emissions. In addition, we compared point measurements with large model grid boxes.

We isolated single grid cells near high fire activity (determined by 5-year average carbonaceous fire aerosol concentrations) to compare daily model with MODIS and MISR satellite AOD (Fig. 2). These locations also corresponded to AERONET stations. For South America, at the Cuiba Miranda station, the DF simulations increased the R^2 from 0.49 to 0.56 for MISR (relative to MF), from 0.21 to 0.25 for MODIS, and from 0.45 to 0.72 for AERONET. For the Mongu station in Africa, there was improvement in the DF simulations from 0.21 to 0.25 for MISR, from 0.11 to 0.16 for MODIS, and from 0.39 to 0.45 for AERONET. Marbel University, in Equatorial Asia, showed no correlations between either satellite and model data. The model simulations of the AERONET AOD data improved from 0.42 to 0.64 for MF to DF, based on only one month of data. Overall, we only saw clear improvements with MISR data at Cuiba Miranda. The differences between MISR and MODIS could be related to the satellite products' spatial resolution (0.5° for MISR vs. 1.0° for MODIS) or the order of magnitude difference in available daily data for the three locations (430 days for MISR versus 3329 days for MODIS).

To elucidate mechanisms driving differences in aerosol concentrations between DF and MF, we investigated whether daily fire emissions are better synchronized with model meteorology than monthly emissions, which, for example, would limit how often fire emissions are released during precipitation events. Note that there were not substantial changes in monthly precipitation totals between DF and MF, due to the meteorology being constrained. Fig. 3 shows the distribution of monthly wet deposition, normalized by total mass concentrations, for BC emitted from biomass burning. The features for OC (not shown) are very similar. All three tropical GFED regions (top row) and smaller analysis regions (bottom row) have more months with lower wet deposition in DF compared to MF (negative values); this effect is most pronounced in Equatorial Asia. These results suggest: 1) the DF run may simulate more intuitive fire emissions transport and removal processes, with increased fire emissions occurring on low precipitation days, leading to reduced wet removal of aerosol particles from the atmosphere and hence longer lifetimes (Tables 3 and 4), and 2) the response to emissions from certain fire types, such as in tropical peatland forests in Equatorial Asia, are more strongly influenced by the temporal resolution of fire emissions. This is partly reflected in the higher DF concentrations found in much of the region, though some parts of it (most of Sumatra) feature decreased DF concentrations (Fig. 1).

3.1.2. *Trace gases*

The difference between DF and MF 2005–09 average surface CO exhibited similar spatial patterns to the carbonaceous aerosol distribution (Fig. 1b). Since aerosols and CO do not share common underlying chemistry or removal mechanisms, the distributions suggest transport-related differences between DF and MF. In boreal North America, Chen et al. (2009) found that using fire emissions finer than monthly resolution tended to increase long-range transport while decreasing both CO and aerosol concentrations near source regions. The changes in 5-year average surface CO between DF and MF were generally within 10%, with a maximum approaching +20% in DF over Borneo and Singapore (Fig. S1). We

Table 2
Linear correlation coefficient (R^2) between 24-h ground-based AERONET observations and model simulations. Italicized results are not statistically significant at the 0.05 level using a Student's *t*-test. Summary rows indicate how many stations showed improvement for DF versus MF, only when MF and DF were both significant and with $R^2 > 0.10$. SHSA = Southern Hemisphere South America, SHAF = Southern Hemisphere Africa, EQAS = Equatorial Asia.

Region	Location	DF	MF	NF
SHSA	Abracos Hill	0.62	0.56	0.048
	Alta Floresta	0.48	0.50	0.12
	Belterra	0.46	0.18	0.14
	Campo Grande	0.52	0.40	0.024
	Cuiba Miranda	0.72	0.45	0.024
	Petrolina Sonda	0.092	0.090	0.073
	Rio Branco	0.41	0.52	0.067
	Santa Cruz	0.59	*0.49*	0.0007
	Santa Cruz Utepsa	*0.50*	*0.56*	0.13
	Sao Paulo	0.24	0.14	*0.024*
	Summary	**5/7 DF > MF**		
SHAF	ICIPE-Mbita	0.048	0.029	0.025
	Ilorin	0.19	0.18	0.087
	Kibale	0.26	0.43	0.078
	Mongu	0.45	0.39	0.053
	Nairobi	0.13	0.11	0.15
	Niamey	0.44	0.44	0.30
	Skukuza	0.23	0.20	0.079
	Summary	**4/5 DF > MF**		
EQAS	Jabiru	0.32	0.32	*0.17*
	Bandung	0.0015	0.018	0.033
	Puspiptek	0.0041	0.070	0.052
	Singapore	0.083	0.044	0.0042
	Bac Lieu	0.15	0.088	0.063
	ND Marbel University	*0.64*	*0.42*	*0.44*
	Songkhla	0.12	0.13	0.088
	Summary	**0/2 DF > MF**		

did not find significant changes in the global CO lifetime or transport (Tables 3 and 4).

There were not significant improvements in CO comparisons with ground observations, except for Bukit Koto Tabang in Equatorial Asia (Table 5). Due to their distance from fire sources, some stations (Cape Point and Ushuaia) also had little improvement over NF. We also performed comparisons with TES satellite CO and O_3 observations. However, because free tropospheric CO and O_3 differences between the two simulations are minimal and applying the TES averaging kernels (e.g. see Voulgarakis et al. (2011)) provides a weighting towards the middle to upper troposphere, there were undetectable differences at multiple levels in the troposphere between the two simulations when compared to TES.

Surface O_3 and OH concentrations largely decreased in all three tropical GFED regions (Fig. 1c and d, and S1). There was less than a 10% decrease in O_3 for the DF versus MF run, and up to 15% decrease for OH. Table 5 shows the negligible effect of the fire emissions dataset on modeled O_3 correlations with station observations. As with CO, several stations did not see any improvement compared to NF. There were negligible changes on O_3 lifetime and transport (Tables 3 and 4). OH concentrations are determined by O_3 levels, but also by water vapor availability and by O_3 photolysis rates (Voulgarakis et al., 2013a). Here, the two latter factors either did not change significantly (water vapor) or changed towards the opposite direction (photolysis rates), suggesting that O_3 decreases drove OH changes. The O_3 decrease may be driven by faster O_3 photolysis rates at low altitudes, but the photolysis changes were small compared with O_3 concentration changes. With aerosol emissions concentrated over shorter time periods in DF, there could be an increase in photolysis rates during non-fire conditions, with less smoke pollution blocking radiation from reaching the surface. Another possible contributing factor is that with MF, fire emissions are released during storms with lightning emissions (including O_3 precursors), causing increased O_3 production. We found that daily aerosol emissions were less affected by wet deposition, which would support fewer fire emissions concurrently emitted during lightning events. This requires further investigation.

3.2. Air quality

Exceedances over WHO ITs showed differences in the DF versus MF simulations depending on both the temporal averaging interval and concentration level. Fig. 4 shows the total 2005–09 exceedances above multiple WHO IT threshold levels for 24-h $PM_{2.5}$, annual $PM_{2.5}$, and 8-h maximum O_3, in each of the three regions of high fire activity (delineated by solid red boxes in Fig. 2a). For 24-h $PM_{2.5}$ (Fig. 4 top row), DF exceedances were consistently higher than MF only at high $PM_{2.5}$ concentrations (>75 $\mu g/m^3$). MF emissions are averaged over an entire month even if fires occur on a few days, limiting model simulations of extreme concentrations. At the lower ITs (25, 37.5, and 50 $\mu g/m^3$), estimated exceedances were often lower with DF because MF showed an increased number of simulated mid-range concentrations, whereas DF has an increased number of the highest concentrations (Fig. 5). The difference between DF and MF annual $PM_{2.5}$ exceedance estimates, (Fig. 4 middle row) were generally smaller than with the 24-h targets. Differences were also small for the O_3 WHO ITs and showed some slight declines with DF (Fig. 4 bottom row), which follows the concentration results described in the previous section.

We assessed the changes in cardiovascular disease mortality attributable to annual $PM_{2.5}$ exposure (Fig. 6). The changes were relatively minor for all tropical regions (which correspond to the high fire activity areas in Fig. 2a). The largest changes, which were still less than 10%, were only observed in years with high fire activity, such as the 2006 fire season in Equatorial Asia. The nonlinear shape of the concentration-response function that is used to estimate mortality dampens the effect of changes in high concentrations on mortality estimates. We also explored changes in daily all-cause mortality due to fire PM_{10} (Ostro, 2004), but since the concentration-response function assumes a linear relationship up to 125 $\mu g/m^3$ and no further increases in risk at higher concentrations, the changes between DF and MF were also small (Fig. S2).

3.3. Radiative forcing

Global 5-year average combined shortwave and longwave radiative forcing was 10% and 6% higher at the top of atmosphere and surface, respectively, in DF versus MF when we considered only the BC tracer from biomass burning (see Shindell et al. (2013a) for an overview of global aerosol radiative forcing). The effect was much smaller when we consider BC as a whole, because there is no change in the other BC components (fossil and bio fuel emissions). The version of the PUCINNI model used in this study did not report OC forcing from biomass burning, but in a previous study, historical total biomass burning forcing calculated with this model indicates good agreement with other models, with a mean estimated global effect of 0 W/m^2 (Shindell et al., 2013a).

Fig. 7 shows maps of the combined shortwave and longwave radiative forcing (DF-MF and DF only) for the surface and top of atmosphere (in 10^{-2} W/m^2) for BC from biomass burning. Relative changes in the forcing were largest in Equatorial Asia ($\sim+75\%$ in DF over much of the region at the top of atmosphere and over 80% north of Sumatra and Borneo at the surface); Africa and South America show mixed changes generally within $\pm30\%$. Changes in atmospheric heating (TOA-surface forcing) followed the observed

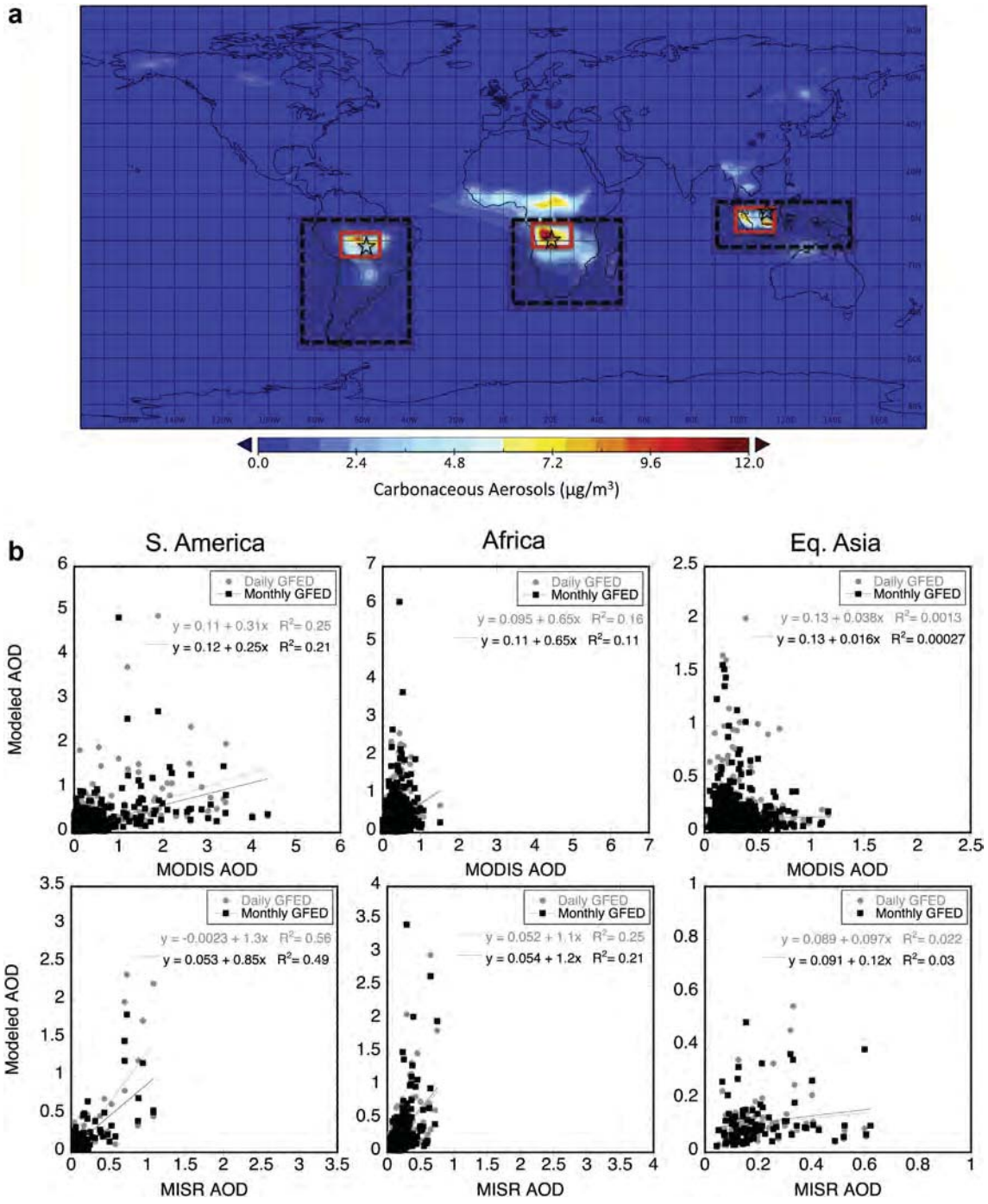

Fig. 2. a) Regions of analysis for model-data intercomparisons. Locations for comparisons of model AOD with MODIS and MISR satellite AOD observations (black stars), GFED basis regions (dotted black boxes) and small target regions for analysis (solid red boxes). Underlying map shows the 2005–09 average carbonaceous surface aerosol concentrations due to fires only, using daily fire emissions. b) Daily mean satellite AOD (MODIS, top row, and MISR, bottom row) versus modeled AOD for 2005–2009. (For interpretation of the references to colour in this figure legend, the reader is referred to the web version of this article.)

TOA patterns (maps not shown). There was little change (~1%) in hemispheric or global O_3 forcing and no change in SO_4 forcing.

4. Discussion

We observed both increases and decreases of aerosol concentrations in response to changing the temporal resolution of fire emissions, though the changes generally support our three hypotheses. Compared with ground-based AERONET observations, we found that correlations between simulated and observed AOD tend to improve with DF over MF (Table 2), but found less improvement when model simulations were compared with satellite AOD. Improvements were more pronounced in South America and Equatorial Asia than savanna-dominated Southern Hemisphere Africa, which is expected from the ability of DF to capture fire events that are concentrated over several days in these biomes. Analysis into the mechanism behind these changes lends support to our hypothesis that the daily fire emissions are better timed with

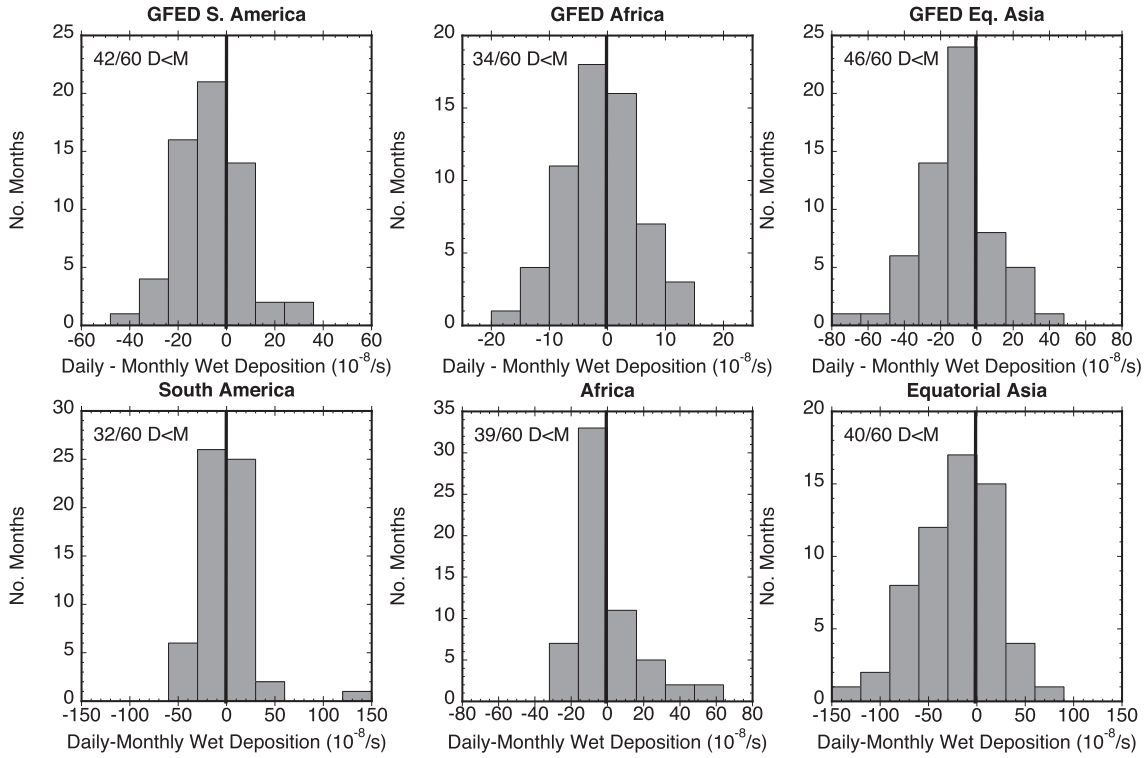

Fig. 3. Difference in monthly wet deposition, normalized by concentrations, for black carbon from biomass burning. Negative values indicate that there was less wet deposition in DF for that month. Locations refer to boxes in Fig. 2a; top row represents GFED regions and bottom row represents smaller target regions.

meteorology. For example, wet deposition of BC was much lower with daily fire emissions (Fig. 3) and the global lifetime was 10% higher (Table 3), suggesting that the fire emissions were not released as frequently during rainy days or were emitted into faster-moving air masses that could carry more emissions to higher altitudes.

The impacts of daily emissions on trace gases were generally smaller, likely due to several interactions in affected chemical processes, and to the longer lifetime of the gases examined compared to aerosols. As with aerosols, we observe both increases and decreases of CO after implementing daily resolution fires (increases in Borneo, Singapore, and western Africa; slight decreases elsewhere), which was similar to the spatial pattern of aerosols but smaller in magnitude. In contrast, O_3 and OH decreased in all tropical source regions, but with relatively small changes. Comparisons to ground-based observations were inconclusive because tropical WDCGG station coverage was much lower than for

Table 3
Global average annual lifetimes for BCB, OCB, CO, and O_3 for DF and MF model runs. CO lifetime is for the tropical troposphere only; O_3 is represented by the global tropospheric burden, in Tg.

Species	DF	MF
BCB	5.2 days	4.7 days
OCB	4.7 days	4.3 days
CO	43.4 days	43.3 days
O_3	221.9 Tg	222.2 Tg

Table 4
BCB, CO, and O_3 fluxes for the small analysis regions outlined in Fig. 2a. Positive u-flux is eastward and positive v-flux is northward.

	Region	U-flux		V-flux	
		DF	MF	DF	MF
BCB (10^{-1} kg/s)	S. America	15.3	15.1	21.6	19.7
	Africa	−21.5	−19.2	−18.0	−16.7
	Eq. Asia	−4.7	−4.5	4.3	2.9
CO (10^3 kg/s)	S. America	0.98	0.97	2.4	2.4
	Africa	−1.6	−1.6	−0.57	−0.54
	Eq. Asia	−0.79	−0.81	0.78	0.78
O_3 (10^3 kg/s)	S. America	4.1	4.1	3.7	3.7
	Africa	−0.72	−0.71	0.27	0.30
	Eq. Asia	−1.4	−1.4	0.002	0.007

Table 5
Linear correlation coefficient (R^2) between 24-h ground-based WDCGG observations and model simulations. Italicized results are not statistically significant at the 0.05 level using a Student's *t*-test. Summary rows indicate how many stations showed improvement for DF versus MF, only when MF and DF were both significant and with $R^2 > 0.10$. SHSA=Southern Hemisphere South America, SHAF=Southern Hemisphere Africa, EQAS = Equatorial Asia.

Species	Region	Location	DF	MF	NF
CO	SHSA	Ushuaia	0.31	0.32	0.16
		Arembepe	*0.36*	*0.37*	0.11
		Summary	**0/1 DF > MF**		
	SHAF	Cape Point	*0.32*	*0.33*	0.32
		Mt. Kenya	0.22	0.26	0.054
		Gobabeb	0.15	0.18	0.11
		Summary	**0/2 DF > MF**		
	EQAS	Bukit Koto Tabang	0.43	0.34	0.073
		Summary	**1/1 DF > MF**		
O_3	SHSA	San Lorenzo	0.27	0.29	0.0071
		Ushuaia	0.60	0.60	0.58
		Summary	**0/1 DF > MF**		
	SHAF	Cape Point	0.61	0.61	0.55
		Mt. Kenya	0.057	0.065	0.014
		Summary	**0/0 DF > MF**		
	EQAS	Danum Valley	0.28	0.28	*0.27*
		Bukit Koto Tabang	0.18	0.21	0.16
		Summary	**0/1 DF > MF**		

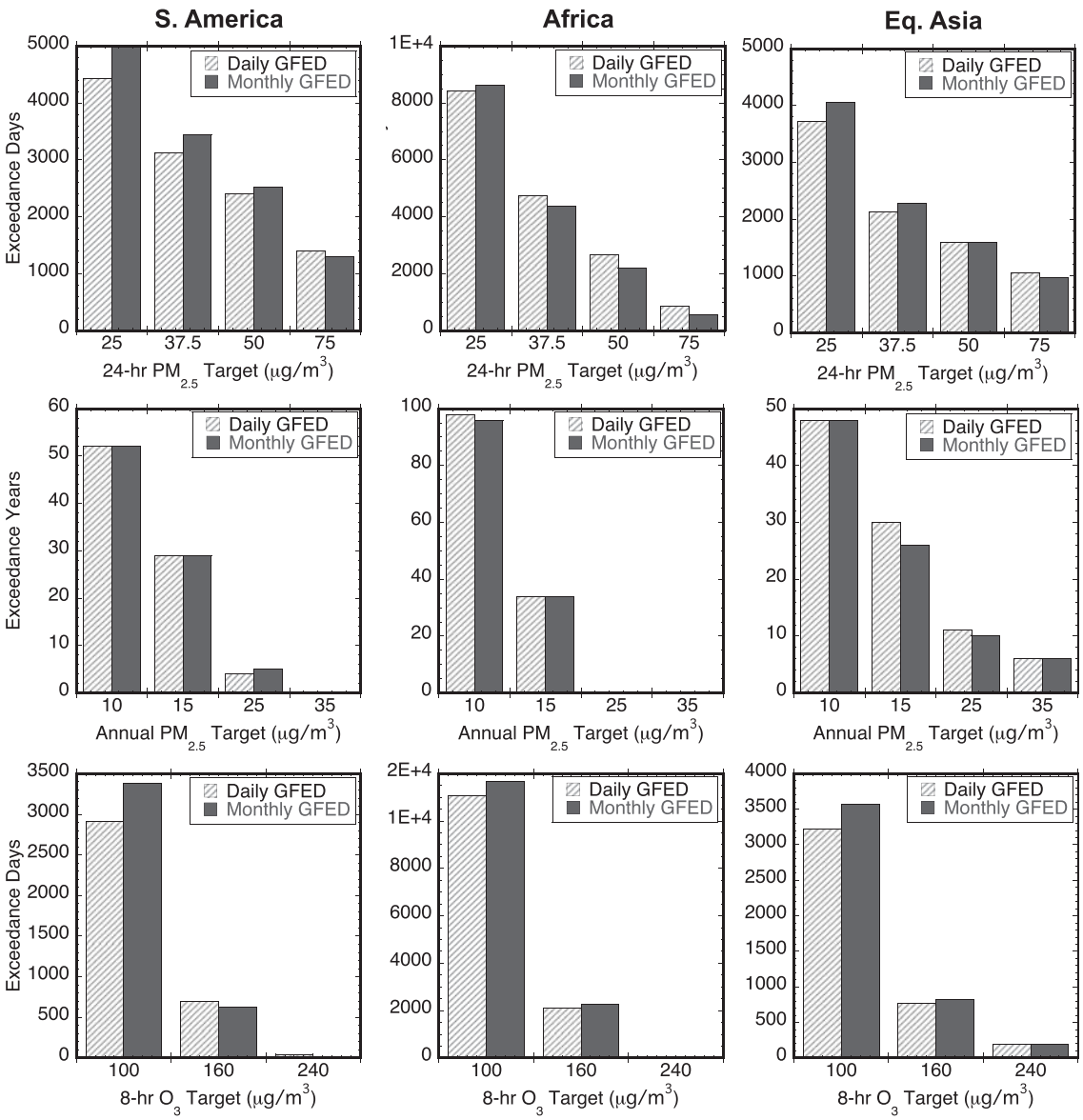

Fig. 4. Accumulated daily exceedances over WHO interim targets for 2005–09, for small target regions shown in Fig. 2a. Top row are exceedances over the 25, 37.5, 50, and 75 μg/m^3 24-h $PM_{2.5}$ targets; middle row are exceedances over the 10, 15, 25, and 35 μg/m^3 annual $PM_{2.5}$ targets; bottom row are exceedances over the 100, 160, and 240 μg/m^3 8-h maximum O_3 targets.

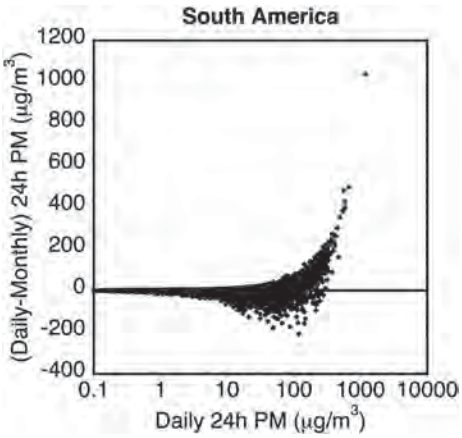

Fig. 5. Difference between 24-h DF and MF (*y*-axis) versus DF $PM_{2.5}$ concentrations (*x*-axis). Note log scale on *x*-axis.

AERONET, which made it difficult to find stations close to fires. This could be due to the stations not collecting measurements during peak fire times during 2005–09, or to the stations being located far enough away from burning regions that either fires did not influence concentrations or the signal was thoroughly mixed before reaching the station.

For public health, the impact of the temporal resolution will depend on the specific endpoint of interest. Overall, $PM_{2.5}$ air quality metrics were more affected by the changes in fire emissions temporal resolution than O_3. DF showed a higher number of exceedance days in all regions for the threshold >75 μg/m^3 $PM_{2.5}$; the increase in extreme concentrations evident in DF is likely strongly influenced by the increase in peak fire emissions (Fig. 5). Monthly average fire emissions cannot resolve these extreme emissions with as much detail (see Fig. 4 in Mu et al. (2011)) and instead have an increased number of mid-range concentrations. While this was important for modeling population exposure to $PM_{2.5}$ above WHO-designated thresholds at 24-h averaging intervals, we did not find substantial differences between the two emissions datasets for

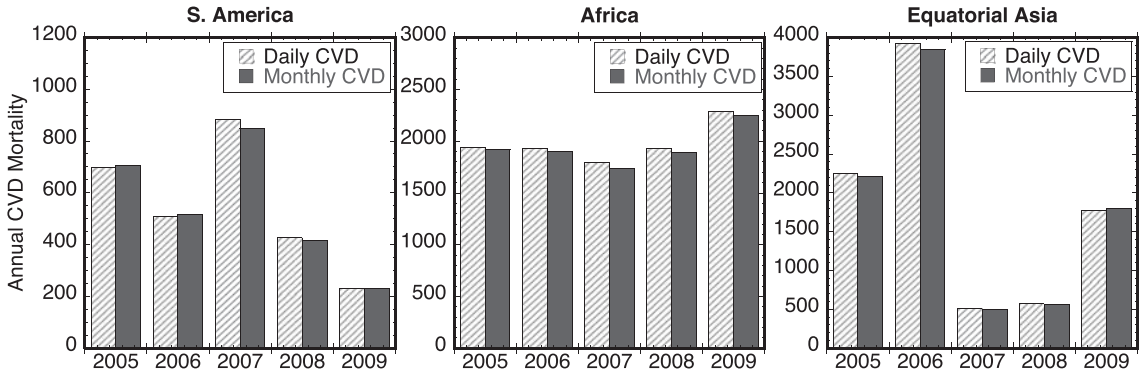

Fig. 6. Annual 2005–09 cardiovascular disease (CVD) mortality due to annual $PM_{2.5}$ exposure to fires-only pollution for DF and MF. Locations correspond to small target regions in Fig. 2a.

threshold exceedances over annual-averaged $PM_{2.5}$, 8-h O_3, or in the $PM_{2.5}$ daily or annual mortality burden. Regardless, many countries, including the United States, determine compliance with air quality standards by calculating the number of days that exceed given thresholds for certain pollutants (http://www.epa.gov/air/criteria.html). Our results suggest that for modeling exceedances over 24-h $PM_{2.5}$ guidelines, it is important to recognize how the fire emissions input dataset itself may modify the determination of compliance for different mitigation or future change scenarios. The magnitude of this effect will be impacted by the temporal resolution of the endpoint and by non-linear response functions, such as those used to estimate mortality.

Resulting changes in radiative forcing estimates could alter model estimates of how fires impact the hydrological cycle and atmospheric heating or cooling, among other effects. There were large regional changes in radiative forcing for biomass burning components of BC (between −30% and +50% in localized areas of Equatorial Asia). These regional changes in atmospheric absorption can strongly influence model representations of changes in local temperature and precipitation.

This analysis showed how the temporal variability of fire emissions could cause uncertainty in modeling the atmospheric impacts of fires. Aerosols were more strongly influenced by the emissions temporal resolution, which can have important effects in understanding how well models reproduce constituent observations, estimating exceedances over air quality thresholds, and predicting regional radiative forcing effects. Our results also suggest the importance of understanding how individual fire events are represented in global models. One related aspect not investigated here is the consistent representation of the fraction of emissions that occur above the boundary layer during different events, and the influence this has on the subsequent transport of

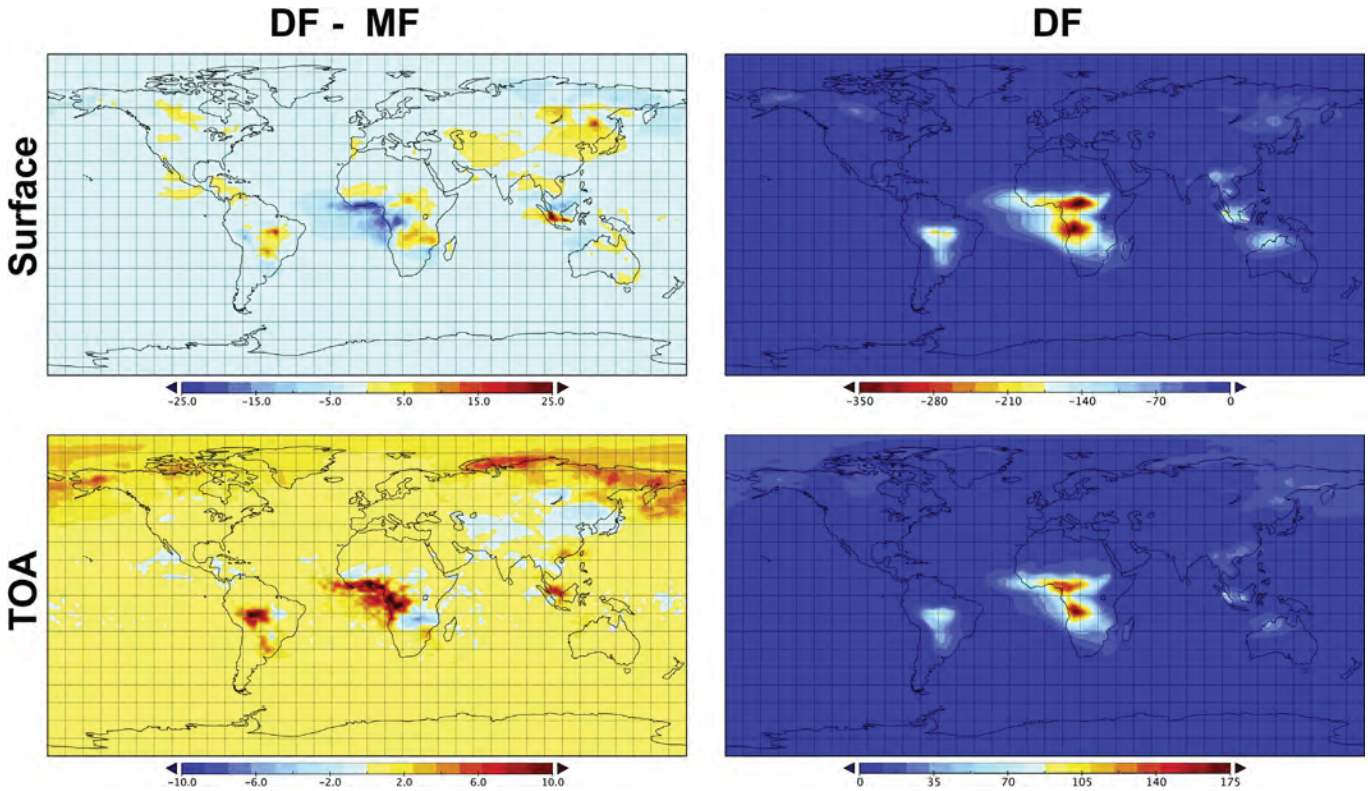

Fig. 7. Radiative forcing (combined shortwave and longwave) for black carbon from biomass burning only at the surface and top of atmosphere (TOA). Units are in 10^{-2} W/m^2.

pollution. In this study, we mixed fire emissions in the boundary layer, since previous work in Indonesia and North America has found that the majority of fire plumes are trapped within stable atmospheric layers (Tosca et al., 2011; Val Martin et al., 2010). However, it would be worth examining the impact of using high temporal resolution injection heights in future global studies. Also, further investigation will explore the robustness of our results to different atmospheric models with multiple spatial resolutions and the sensitivity to using diurnal resolution fire emissions.

Acknowledgments

The authors would like to thank Ruth DeFries for helpful discussions regarding this work. We acknowledge funding support from the NSF Graduate Research Fellowship Program, NASA MAP and ACMAP programs, the NASA High-End Computing (HEC) Program through the NASA Center for Climate Simulation (NCCS), and NASA grant NNX11AF96G.

Appendix A. Supplementary data

Supplementary data related to this article can be found at http://dx.doi.org/10.1016/j.atmosenv.2014.02.039.

References

Andreae, M.O., Merlet, P., 2001. Emission of trace gases and aerosols from biomass burning. Global Biogeochemical Cycles 15 (4), 955–966.
Atwood, S.A., et al., 2013. Analysis of source regions for smoke events in Singapore for the 2009 El Niño burning season. Atmospheric Environment 78, 219–230.
Baccini, A., et al., 2012. Estimated carbon dioxide emissions from tropical deforestation improved by carbon-density maps. Nature Climate Change 2 (3), 182–185.
Boersma, K.F., et al., 2008. Intercomparison of SCIAMACHY and OMI tropospheric NO_2 columns: observing the diurnal evolution of chemistry and emissions from space. Journal of Geophysical Research 113 (D16S26).
Chen, Y., et al., 2009. The sensitivity of CO and aerosol transport to the temporal and vertical distribution of North American boreal fire emissions. Atmospheric Chemistry and Physics 9 (17), 6559–6580.
CIESIN, 2005a. Gridded Population of the World Version 3 (GPWv3): Population Grids. Socioeconomic Data and Applications Center (SEDAC), Columbia University, Palisades, NY. Palisades, NY. Available at: http://sedac.ciesin.columbia.edu/gpw.
CIESIN, 2005b. Gridded Population of the World: Future Estimates, 2015 (GPW2015): Population Grids. Socioeconomic Data and Applications Center (SEDAC), Columbia University, Palisades, NY. Palisades, NY. Available at: http://sedac.ciesin.columbia.edu/gpw.
Duncan, B.N., et al., 2003. Interannual and seasonal variability of biomass burning emissions constrained by satellite observations. Journal of Geophysical Research 108 (D2), 4100.
Giglio, L., et al., 2009. An active-fire based burned area mapping algorithm for the MODIS sensor. Remote Sensing of Environment 113 (2), 408–420.
Giglio, L., et al., 2010. Assessing variability and long-term trends in burned area by merging multiple satellite fire products. Biogeosciences 7, 1171–1186.
Guenther, A., et al., 1995. A global model of natural volatile organic compound emissions. Journal of Geophysical Research 100 (D5), 8873–8892.
Guenther, A., et al., 2006. Estimates of global terrestrial isoprene emissions using MEGAN (Model of Emissions of Gases and Aerosols from Nature). Atmospheric Chemistry and Physics 6, 3181–3210.
Heald, C.L., et al., 2003. Biomass burning emission inventory with daily resolution: application to aircraft observations of Asian outflow. Journal of Geophysical Research 108 (D21), 8811.
Holben, B., et al., 1998. AERONET—A federated instrument network and data archive for aerosol characterization. Remote Sensing of Environment 66 (1), 1–16.
Kaiser, J.W., et al., 2012. Biomass burning emissions estimated with a global fire assimilation system based on observed fire radiative power. Biogeosciences 9 (1), 527–554.
Koch, D., Schmidt, G.A., Field, C.V., 2006. Sulfur, sea salt, and radionuclide aerosols in GISS ModelE. Journal of Geophysical Research 111 (D06206).
Lamarque, J.-F., et al., 2010. Historical (1850–2000) gridded anthropogenic and biomass burning emissions of reactive gases and aerosols: methodology and application. Atmospheric Chemistry and Physics 10 (15), 7017–7039.
Langmann, B., et al., 2009. Vegetation fire emissions and their impact on air pollution and climate. Atmospheric Environment 43, 107–116.
Lee, Y.H., et al., 2013. Evaluation of preindustrial to present-day black carbon and its albedo forcing from Atmospheric Chemistry and Climate Model Intercomparison Project (ACCMIP). Atmospheric Chemistry and Physics 13 (5), 2607–2634.
Mu, M., et al., 2011. Daily and hourly variability in global fire emissions and consequences for atmospheric model predictions of carbon monoxide. Journal of Geophysical Research 116 (D24303).
Ostro, B., 2004. Outdoor Air Pollution: Assessing the Environmental Burden of Disease at National and Local Levels. World Health Organization, Geneva.
Pope, C.A., et al., 2011. Lung cancer and cardiovascular disease mortality associated with ambient air pollution and cigarette smoke: shape of the exposure-response relationships. Environmental Health Perspectives 119, 1616–1621.
Price, C., Penner, J., Prather, M., 1997. NO_x from lightning 1. Global distribution based on lightning physics. Journal of Geophysical Research 102 (D5), 5929–5941.
Rayner, N.A., et al., 2003. Global analyses of sea surface temperature, sea ice, and night marine air temperature since the late nineteenth century. Journal of Geophysical Research 108 (D14), 4407.
Reid, J.S., et al., 2009. Global monitoring and forecasting of biomass-burning smoke: description of and lessons from the fire locating and modeling of burning emissions (FLAMBE) program. IEEE Journal of Selected Topics in Applied Earth Observations and Remote Sensing 2 (3), 144–162.
Rienecker, M.M., et al., 2011. MERRA: NASA's modern-era retrospective analysis for research and applications. Journal of Climate 24, 3624–3648.
Shindell, D.T., et al., 2013a. Radiative forcing in the ACCMIP historical and future climate simulations. Atmospheric Chemistry and Physics 13 (6), 2939–2974.
Shindell, D.T., et al., 2013b. Interactive ozone and methane chemistry in GISS-E2 historical and future climate simulations. Atmospheric Chemistry and Physics 13 (5), 2653–2689.
Tosca, M.G., et al., 2011. Dynamics of fire plumes and smoke clouds associated with peat and deforestation fires in Indonesia. Journal of Geophysical Research 116 (D08207).
UN, 2011. World Population Prospects: the 2010 Revision, CD-ROM ed. Department of Economic and Social Affairs Population Division.
Val Martin, M., et al., 2010. Smoke injection heights from fires in North America: analysis of 5 years of satellite observations. Atmospheric Chemistry and Physics 10, 1491–1510.
van der Werf, G.R., et al., 2008. Climate regulation of fire emissions and deforestation in equatorial Asia. Proceedings of the National Academy of Sciences 105, 20350–20355.
van der Werf, G.R., et al., 2010. Global fire emissions and the contribution of deforestation, savanna, forest, agricultural, and peat fires (1997–2009). Atmospheric Chemistry and Physics 10 (23), 11707–11735.
Voulgarakis, A., et al., 2011. Global multi-year O_3–CO correlation patterns from models and TES satellite observations. Atmospheric Chemistry and Physics 11 (12), 5819–5838.
Voulgarakis, A., et al., 2013a. Analysis of present day and future OH and methane lifetime in the ACCMIP simulations. Atmospheric Chemistry and Physics 13, 2563–2587.
Voulgarakis, A., Shindell, D.T., Faluvegi, G., 2013b. Linkages between ozone-depleting substances, tropospheric oxidation and aerosols. Atmospheric Chemistry and Physics 13 (9), 4907–4916.
Wang, J., Christopher, S.A., 2006. Mesoscale modeling of Central American smoke transport to the United States: 2. Smoke radiative impact on regional surface energy budget and boundary layer evolution. Journal of Geophysical Research 111 (D14S92).
Wiedinmyer, C., et al., 2011. The Fire INventory from NCAR (FINN): a high resolution global model to estimate the emissions from open burning. Geoscientific Model Development 4 (3), 625–641.
World Health Organization, 2006. WHO Air Quality Guidelines for Particulate Matter, Ozone, Nitrogen Dioxide and Sulfur Dioxide. World Health Organization, Geneva.
World Health Organization, Department of Measurement and Health Information (WHO), 2011. Death Estimates for 2008 by Cause for WHO Member States. Available at: http://www.who.int/healthinfo/global_burden_disease/estimates_country/en/index.html.
Wu, L., Su, H., Jiang, J.H., 2011. Regional simulations of deep convection and biomass burning over South America: 2. Biomass burning aerosol effects on clouds and precipitation. Journal of Geophysical Research 116 (D17).